Constitutive Properties of Faults With Simulated Gouge

JAMES H. DIETERICH

U.S. Geological Survey, Menlo Park, California 94025

Direct shear experiments with a layer of simulated fault gouge consisting of crushed and sieved Westerly Granite sandwiched between intact blocks of Westerly Granite show a variety of competing time-, velocity-, and displacement-dependent effects similar to previous friction observations for slip on initially clean surfaces (Dieterich, 1979*a*). Gouge strength increases by approximately the logarithm of the time that the driving ram is held stationary. A change of sliding velocity results in an immediate but transient change in strength and a displacement-dependent residual change of strength. The transient and residual velocity-dependent effects result from the competition between a direct velocity-dependent process that operates continuously during slip and a process inversely dependent on velocity that becomes fully effective only following a finite displacement d_r at a specific velocity. The residual velocity-dependent effect results in strength changes that are of the same or opposite sign as the velocity change depending on the relative magnitude of the competing processes. The experiments with gouge show variations in the magnitude and sign of the residual velocity effect that appear to be correlated with the rate of comminution of the gouge. The displacement dependency measured by the parameter d_r scales by both gouge particle size and roughness of the surface in contact with the gouge. The parameter d_r is insensitive to thickness of the gouge layer, indicating that deformation in the gouge is highly localized, probably at the gouge-rock interface. A constitutive law of the general type proposed by Dieterich (1979*a*) adequately represents the range of behavior seen in these experiments. Because experimental results arise from interactions between the fault and the laboratory apparatus, a simple deterministic spring-slider numerical model that uses the constitutive law is employed to simulate the experiments. This single model reproduces in detail the full range of effects seen in these laboratory experiments. In addition, it produces a previously observed dependence of mode of slip (stick slip, stable slip, or oscillatory slip) on machine stiffness, normal stress, and the parameter d_r. Accelerating premonitory slip precedes all unstable slip events.

Introduction

Active faults exhibit a variety of deformation phenomena, the most obvious, of course, being earthquake slip. In addition, faults may undergo decelerating postseismic slip (afterslip), long-term stable slip (fault creep) in the absence of earthquake instability, and perhaps slow preseismic slip. Fault creep may be of the nearly constant velocity type, or it may be characterized by repeated alternating episodes of slow stable slip and rapid creep events. Parallel behavior has been demonstrated in laboratory experiments using simulated faults. Significantly, accentuation or inhibition of different slip characteristics can be brought about by changing the physical conditions of the experiment. An example that illustrates this point is the demonstration that a change of the stiffness of the laboratory apparatus is sufficient to alter the mode of slip [*Dieterich*, 1979*a*]. Low stiffness favors unstable fault slip, and high stiffness results in stable slip. Other factors such as normal stress, strain rates, and surface characteristics of the fault also have been shown to significantly affect the mode of slip.

This range of slip behavior, in which the mode of slip can be changed simply by altering the characteristics of the loading apparatus, points to the inescapable conclusion that faults possess fairly complicated constitutive properties and that the observed mode of slip in both laboratory experiments and in nature can be regarded as the result of interactions between the constitutive properties of the fault and the total mechanical system that stresses the

fault. In this context it seems reasonable to conclude that understanding of active faulting and the attainment of such practical goals as the prediction of the time and location of earthquake slip depend in large part on understanding both these factors.

Dieterich [1979*a*] discusses some of the general features of constitutive behavior implied by gross observations of modes of slip and within a general framework presents a specific formulation for a fault constitutive law. This is based on a limited series of experiments for slip on initially clean surfaces of granite. The general constitutive model at the minimum provides a qualitative explanation for the range of behavior observed, and the specific model accounts for the limited experimental data in detail. The principal purpose of the present study is to obtain experimental results for the more appropriate case of a fault with a layer of finely comminuted rock fragments, i.e., gouge, and to explore the extent to which the constitutive model can be applied to faults with simulated gouge.

A number of studies of faults with simulated gouge have been described in the literature [*Engelder et al.*, 1975; *Byerlee and Summers*, 1976; *Summers and Byerlee*, 1977; *Weeks and Byerlee*, 1978; *Byerlee et al.*, 1978; *Logan*, 1979]. In most of these studies it is difficult to extract specific quantitative constitutive parameters, because the measurements were designed to answer other questions. However, there are direct parallels between the modes of slip seen in the different gouge experiments and rock friction experiments without gouge. This leads one to expect analogous, if not quantitatively identical, constitutive properties for gouge layers and for rock friction.

Experimental Procedure

The experimental phase of this study examines the relationships between various physical parameters of simulated gouge layers and the response of the fault as a function of stress, displacement, and time when subjected to different types of load histories. The simulated gouge material used here consists of crushed and sieved Westerly Granite placed between blocks of intact Westerly Granite. Parameters that were varied are roughness of the rock surface in contact with the gouge, gouge thickness, and the size fractions of the gouge particles in the starting material. Surfaces with different roughnesses were prepared in a uniform manner by hand-lapping the surfaces using either 60-90, 240, or 600 mesh silicon carbide abrasive to produce surfaces designated throughout this paper as rough, medium, or fine, respectively. For identically prepared surfaces, *Dieterich* [1979*a*] gives surface roughnesses that were measured using a profilometer. Initial gouge layer thicknesses of 0.5 mm, 1.0 mm, and 2.0 mm were controlled using shims of appropriate thickness that were removed after the gouge and blocks were in place. Three particle size groups were prepared by sieving the crushed granite: (1) all size fractions of <250 μm (see Figure 1 for histogram), (2) all size fractions of <85 μm, and (3) the fraction consisting of 125-250 μm.

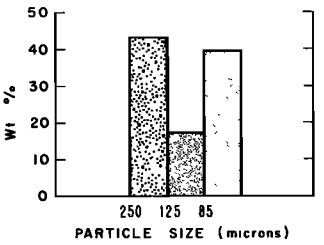

Fig. 1. Histogram of the gouge particle sizes in the starting material <250 μm.

The sample assembly consists of a three-block, sandwich type direct shear configuration described previously [*Dieterich*, 1972] and shown schematically in Figure 2. Prior to loading, the loose, crushed granite is held in place using cellophane tape. The sample assembly includes a modification suggested by A. Ruina. Namely, the inner block has twice the thickness of the outer blocks instead of the previously used equal thicknesses for all blocks. The purpose of this geometry is to reduce differences in the vertical elastic displacements within the blocks induced by the vertical load. With these dimensions the vertical elastic displacements are approximately the same for the inner and outer blocks. This configuration reduces possible slip gradients that would arise from changes in the vertical load.

With this type of direct shear arrangement the vertical and horizontal hydraulic rams independently control the shear and normal stresses, respectively, on the sliding planes. Because of the large number of possible combina-

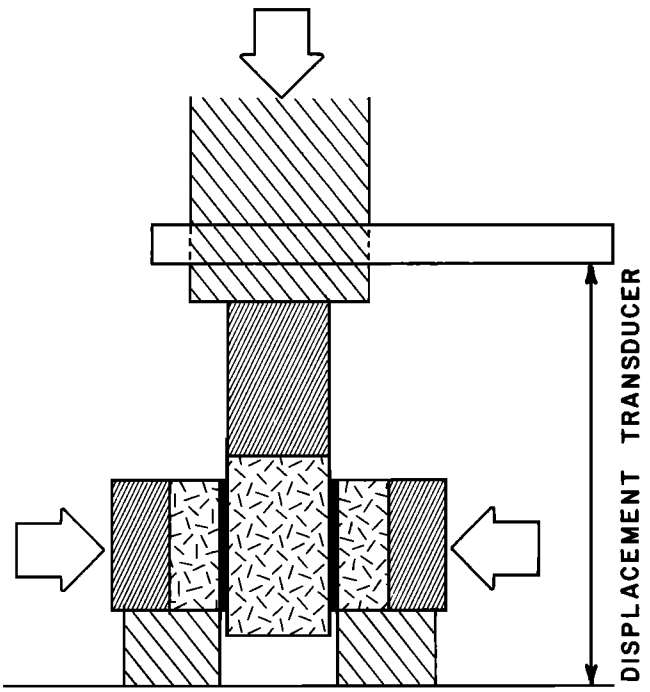

Fig. 2. Diagram of the sample assembly. The dimensions of the sliding surface are 5.0 cm × 5.0 cm.

tions involving surface roughness, gouge thickness, and particle size to be tested, all experiments were conducted at a single normal stress: 10.0 MPa (100 bars). Normal stress was held constant during each test through the use of a hydraulic accumulator. Motion of the vertical ram was generally servo-controlled on displacement using a high-speed servo control valve. Reference signals for the servo controller were supplied from a computer, permitting preprograming of the somewhat complicated velocity histories required for many of the experimental runs. Displacement feedback signals were obtained from a displacement transducer that spanned the sample. One end of the transducer was anchored on the loading column between the sample and the hydraulic cylinder, and the other end was mounted on the base that supports the sample assembly (see Figure 2). Resolution of displacements by the servo controller is variable, depending on amplifier gains and total displacement range. In all cases presented here it is at least as good as 0.2 μm and in most cases at least 0.1 μm. Although the servo valve has a response rate that can approach 1.0 KHz, mechanical resonance of the apparatus requires low-pass filtering of the feedback signal to remove frequencies above 30–40 Hz. Below those frequencies the effective stiffness of the vertical loading system expressed as shear stress at the slip surfaces divided by displacement was measured to be 650 MPa/cm.

Three types of tests were systematically conducted for the different combinations of gouge parameters: constant velocity, multiple velocity, and time dependence tests. The constant velocity tests were run at 2.5 μm/s and were done to examine the overall form of the stress/displacement curves and to permit reasonably direct comparisons to be made for the control of strength by the fault parameters. In the multiple-velocity tests the velocity was held constant for a predetermined displacement, then abruptly changed by a factor of 10, held constant for another displacement interval, then changed again, and so on. Slip velocities used for these tests were 0.25, 2.5, and 25.0 μm/s. The purpose of the multiple-velocity tests was to look for variations of strength as a function of velocity as seen in the earlier friction experiment of *Dieterich* [1979*a*]. Those earlier findings demonstrated two competing velocity effects. For time dependence tests, constant velocity slip is interrupted at specified displacements where the control displacement is held at zero for a specified time interval, followed by resumption of slip at constant velocity. Slip velocities of 2.5 μm/s and hold times of 1000, 100, 10, and 1 s were employed. The purpose of the time dependence test was to quantify the increase of strength with time of nominally stationary contact that was found to be closely related to the velocity dependence and is an essential part of the stick slip process [*Dieterich*, 1978*a*].

In addition, a few constant stress creep tests were tried. For these tests the shear stress was held constant at successively higher levels for an interval of 30 min, then increased to a higher level. The principal motivation for the creep experiments was to see if these measurements at 10.0-MPa normal stress could be related to the creep measurements reported by *Solberg et al.* [1978] at confining pressures to 450 MPa.

Experimental Results

In general, these experiments display time, velocity, and displacement effects that qualitatively agree with the effects reported by *Dieterich* [1979*a*] for friction of initially clean gouge-free surfaces. Quantitatively, these results show some differences from the previous experiments. Additionally, there are some features not specifically represented by the constitutive formulation of *Dieterich* [1979*a*]. The differences between the gouge-free and simulated gouge experiments may have significant implications for applications to natural faults and point to some difficulties that may be encountered in assessing the relevance to natural faulting of some types of experiments reported in the literature.

Condition of Gouge Following the Tests

During a test the gouge layer becomes compacted, and when examined macroscopically or using a hand lens, the gouge either displays a streaked and polished interface with the granite block or it contains well-defined oblique parting planes, or both. If present, the streaking and polishing at the interface indicate concentrated shear in a narrow zone adjacent to the rock. The streaking arises from mafic minerals that consisted originally of individual fragments that have been finely broken up and dragged out along the shear zone. Polishing of the rock surfaces also gives evidence for concentrated shear at the interface between the gouge and the intact rock. In some cases the gouge adheres very strongly to the rock with the result that the streaking cannot be observed, but when the adhering gouge is scraped away, the underlying rock exhibits a polishing down of the original roughness. The oblique parting planes apparently experienced shear also because mafic minerals could be seen to have been dragged out along these surfaces. These features correspond to the shear zones at the gouge-rock interface and the oblique shear planes previously documented in detail by the microscopic studies of deformed simulated gouge [*Tchalenko*, 1970; *Byerlee et al.*, 1978; *Logan*, 1979]. The oblique shears are consistently oriented at a low angle to both the gouge layer and the stress vector acting on the sliding surface as defined by the shear and normal stress. *Tchalenko* [1970] and *Logan* [1979] equate these features to Riedel shears. These features clearly provide some clues concerning the deformation process in the gouge layers. Although there must be some uncertainty in the present interpretations because a microscope was not used for the observations, it is very evident that the roughness of the interface and the particle dimensions of the gouge exert a strong control on the relative development of the shear structures. The most strongly polished and streaked surfaces along the gouge-rock interface were consistently seen with the coarsest

gouge size fractions and the finely ground surfaces. Those combinations of parameters also produced the weakest development of the oblique shears. For the case of the coarsest gouge (125-250 μm) in contact with finely ground surfaces, no oblique shears could be seen, and the surfaces were polished, indicating that most deformation was concentrated slip at the gouge-rock interface. The oblique shears became more conspicuous as the roughness increased and the particle size was decreased. In addition, the oblique shears became more closely spaced as the gouge thickness was reduced.

The histograms of Figure 3 give the final size distributions for the gouge that initially consisted entirely of the 125- to 250-μm size fraction. Note that the greatest size reduction is found with the 0.5-mm layer in contact with the coarse surface and the least reduction in particle size is the 0.5-mm and 2.0-mm layers in contact with the finely ground surface. The former case had the strongest development of oblique shears, and the latter had no visible oblique shears and very prominent streaking and polish at the contact of the gouge with the rock.

In summary, the observations are consistent with the interpretation that fine interfaces enhance the development of concentrated shear zones at the contact of the gouge with the intact rock and reduce the development of the oblique shears. Rough surfaces enhance the development of oblique shears and result in greater deformation within the gouge layer as shown by greater grain size reduction in comparison to fine surfaces. Similarly, thin layers of gouge compared to thick layers result in more intense deformation within the gouge layer and show most highly developed oblique shears and greatest reduction in grain size.

Form of the Stress Versus Displacement Curves

When loaded at a constant velocity (2.5 μm/s), the stress plotted as a function of displacement usually shows an initial peak followed first by slow displacement weakening for 0.5 to 5.0 mm of slip and then stabilization at a residual strength, which does not change or increases very slowly with additional displacement (Figure 4). In approximately 20% of the experiments the strength displays an asymptotic increase to the residual value without passing through a peak. Neither the occasional absence of the large-scale displacement weakening nor the displacement over which the weakening occurs appears to correlate with interface roughness, gouge thickness, or gouge particle size. The coarsest gouge (125-250 μm) consistently showed a less pronounced peak than the other size fractions.

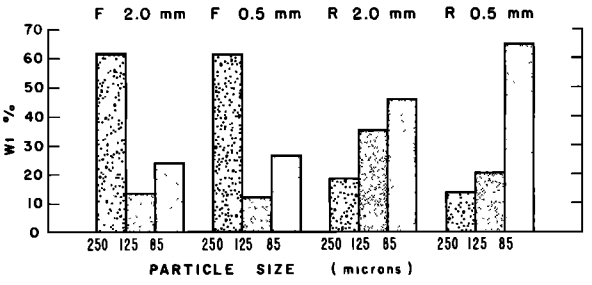

Fig. 3. Particle size histograms of the initial 125- to 250-μm gouge following deformation. The rough and fine interfaces are designated R and F, respectively. Layer thicknesses are 0.5 mm and 2.0 mm.

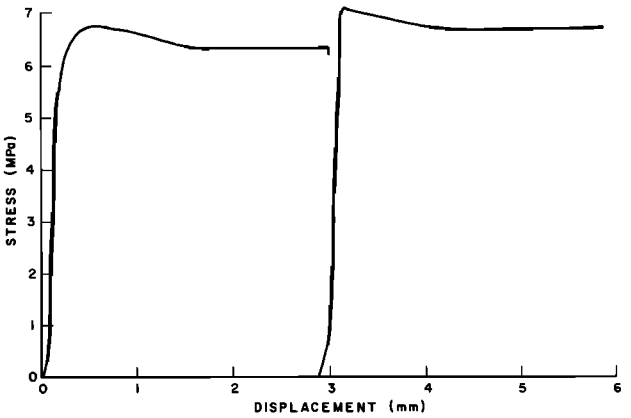

Fig. 4. Shear stress versus displacement for a 1-mm gouge layer consisting of the <250-μm size fraction and rough interface. Sliding velocity is 2.5 μm/s.

Cycling of the shear stress to zero, even momentarily, after reaching the residual strength, acts to restore the peak in the stress-displacement curves (Figure 4). As seen in Figure 4, the cycling and/or the accompanying increase in total displacement results in an increase in the peak and residual strength. The slow increase in residual strength with displacement probably arises from increased comminution of the gouge fragments leading to better packing of the gouge particles. The relationship of the establishment of the transient peak strength to stress cycling probably involves gross rearrangement of the gouge fragments when the shear stress is dropped, possibly by the collapse of dilatant pore volume. The large-scale displacement weakening might then be related to the localization process whereby distinct slip planes become established in the gouge or at the gouge-rock contact. This interpretation is supported by the observations of *Tchalenko* [1970], *Logan* [1979], and *Dengo and Logan* [1979], who report similar stress-displacement curves. In those studies, oblique shears (Riedel shears) began to form at the peak strength, and the development of layer-parallel shears marked the beginning of slip at the residual strength.

The magnitudes of the residual strength plotted as a function of the gouge parameters are given in Figure 5. Throughout this paper, strength is expressed as the ratio of shear stress τ to normal stress σ (i.e., coefficient of friction μ). The letters R, M, and F designate rough, medium, and fine surface roughnesses, respectively, prepared by the lapping procedure noted above. As evident from Fig-

ure 5, gouge thickness, particle size, and perhaps to a lesser extent surface roughness significantly affected the final residual strength. Gouge with size fractions of <85 μm gives greater strength than gouge with size fractions of <250 μm, which has greater strength than the 125- to 250-μm gouge. Hence strength increases with the relative amount of the fine particle size fraction. These relationships of strength with gouge thickness and surface roughness correlate with the observations described above that relate the development of shear structures and grain size reduction. This suggests that strength is partially controlled by the amount or perhaps rate of comminution of the gouge. Hence experimental factors that are associated with enhancement of the development of oblique shears and increased comminution are also associated with increased shear strength. The slow increase of the residual strength with displacement noted above supports this interpretation, as do the observations of grain size reduction. In Figure 3, note that the greatest size reduction is found with the 0.5-mm gouge with the rough interface, which also has the highest strength of the 125- to 250-μm gouge experiments. Conversely, the 2.0-mm layer with a fine interface shows the least size reduction and the lowest strength. From these experimental data alone it cannot be determined unequivocally if the comminution process itself is directly linked to higher strength or if the shear strength is more directly linked to grain size which is changed by comminution. The large-scale displacement weakening which is apparently associated with the localization of slip and possibly reductions in rate of comminution suggests a possible direct dependence of strength on comminution.

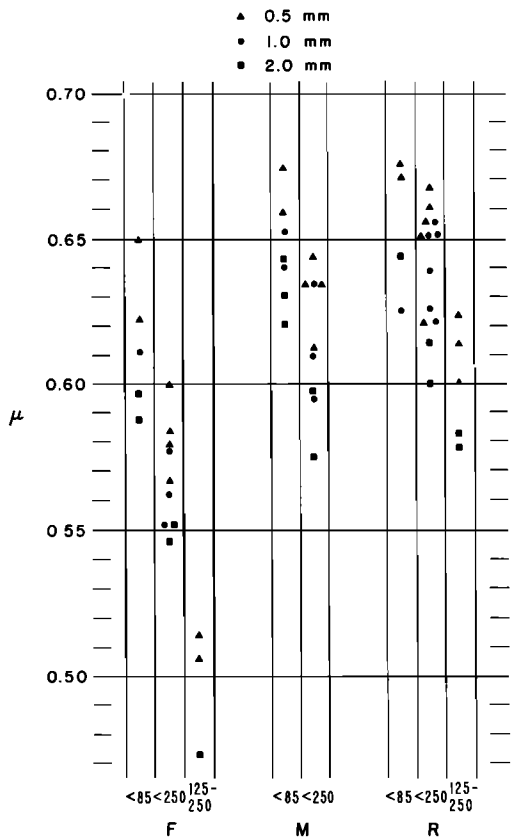

Fig. 5. Residual strength for slip at 2.5 μm/s. The squares indicate 2-mm layers, circles indicate 1-mm layers, and the triangles indicate 0.5-mm layers. R, M, and F refer to rough, medium, and fine surfaces, respectively.

Velocity Dependence

A step change of velocity results in transient and residual changes in strength that qualitatively resemble the features reported previously [*Dieterich*, 1979*a*] for the velocity-dependent slip on ground surfaces of granite. As shown by *Dieterich* [1979*a*], these two types of velocity dependence are distinct and apparently reflect competing underlying mechanical processes. Depending on the type of test, the different processes may appear relatively more or less important. The example given in Figure 6 is representative and illustrates the types of strength and displacement features observed for step changes in velocity. In general, if sliding at a constant velocity has proceeded for a sufficient distance for the strength to have stabilized at a residual value, an abrupt increase of velocity produces an immediate increase in strength followed by a decay in strength with displacement to a new residual value. The new residual strength is usually less than the residual strength for the previous slower sliding velocity. Conversely, an abrupt decrease of the slip velocity results in an immediate drop in strength followed by a displacement dependent rise in strength to a new residual strength that is greater than the previous strength. Hence there are two velocity-dependent effects. The first appears as a direct but transient velocity dependence; and the second, which is generally an inverse dependence with velocity, becomes fully evident only after a finite amount of slip has occurred. Throughout this paper the two types of velocity dependence will be referred to as the transient velocity effect and residual velocity effect. It must be emphasized here that this terminology is intended to describe the character of the observations and not the character of the

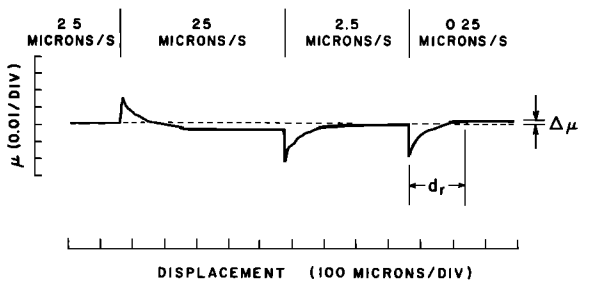

Fig. 6. Shear stress versus displacement showing the typical effect of changes of slip velocity. The gouge is 1-mm thick, <250 μm in contact with rough surfaces.

underlying mechanisms. In fact, the jump in strength that marks the onset of the transient velocity effect is probably the result of a process related to comminution that operates continuously during slip. The reason for the decay of the strength jump with displacement giving the residual velocity effect is that other competing processes require a finite displacement to become fully evident.

Figure 6 defines parameters used to characterize the observations. The displacement required to reach fully the residual value following a factor of 10 change of velocity is designated as d_r. In the previous studies of *Dieterich* [1978*a*, 1979*a*, *b*] this experimentally observed parameter was designated d_c. However, d_c was also used directly as a constitutive parameter. Although principally controlled by constitutive properties, it is now clear that d_r also reflects some effects due to machine interactions. In this paper, d_r refers to the experimental observations, and d_c is retained to represent the related but not identical constitutive parameter. In Figure 7 the parameter B is the slope of the strength change $\Delta\mu$ with the logarithm of the change of velocity from V_1 to V_2:

$$B = \Delta\mu/\log_{10}(V_1/V_2) \quad (1)$$

For the initial series of tests the velocity was changed only after the strength had stabilized at a residual value following the peak strength and gross displacement weakening described above. This preconditioning generally required 2.5–5.0 mm of slip. For those measurements the parameter B is negative, indicating that positive changes of velocity produced a decrease in residual strength. A summary of the residual velocity dependence B for the various combinations of parameters is given by Figure 7. The most striking feature of Figure 7 is the relationship between B and surface roughness. Thickness and particle size show no systematic relationship to B within the scatter of the observations. The dependence of B on surface roughness indicates a possible connection with the observations noted above that relate surface roughness to the development of oblique and contact shears, the amount of grain size reduction in the gouge, and the magnitude μ. In comparison to fine surfaces the rough interfaces enhance the development of oblique shears, result in greater comminution of the gouge, have higher values of μ, and produce less negative values for the parameter B. This suggests that the process that gives less negative values of B is related to comminution processes in the gouge.

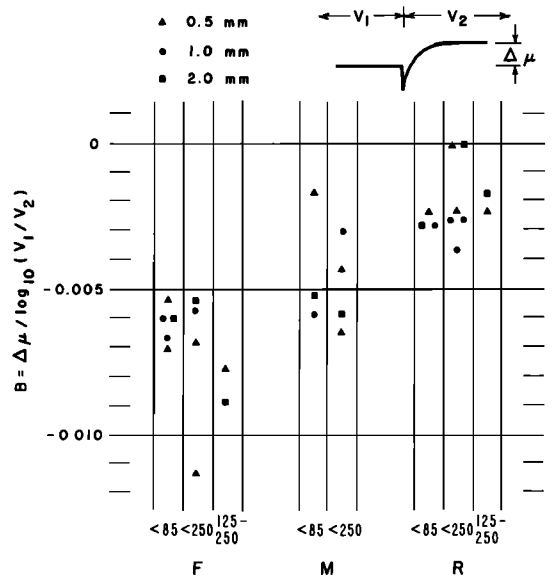

Fig. 7. Summary of the residual velocity dependence. All measurements followed at minimum 2.5 mm of slip to precondition the gouge.

Overall, the result that B is negative agrees with the findings for residual velocity dependence for friction of initially clean granite surfaces [*Dieterich*, 1978*a*, 1979*a*] and for corundum on granite [*Scholz and Engelder*, 1976]. However, *Solberg and Byerlee* [1979] found a positive velocity dependence in triaxial experiments with a layer of crushed Westerly Granite along an inclined saw cut in a cylinder of Westerly Granite. There are two possible explanations for the different results seen in the latter experiments: First, fundamentally different mechanisms may operate at the higher confining pressures used for those experiments, or second, some aspect of the sample preparation or experimental procedure may result in the selective enhancement of one of the competing mechanisms that underly the rather complicated transient and residual velocity-dependent effects seen for the present experiment. The results obtained here favor the latter explanation. Figure 8 shows the results of a test that is similar to the usual velocity test except the velocity was cycled from the beginning of the run instead of first presliding the sample until the strength stabilized. This procedure more closely corresponds to the procedure used by *Solberg and Byerlee* [1979], who also cycled the velocity from the beginning of the run. Note that the velocity dependence as defined by parameter B is initially very strongly positive, as found by *Solberg and Byerlee* [1979] for the triaxial tests, but that B decreases with total displacement and stabilizes at a negative value. Hence the absence of preconditioning in the triaxial experiments appears to be an important causative factor for the positive velocity dependence. Because the purpose of these tests is to obtain better insight into the constitutive properties of natural faults that generally have very large displacements compared to laboratory tests, it was decided to conduct all subsequent velocity tests after first presliding the blocks to reach the residual strength. Under these conditions the velocity dependence appears to be relatively insensitive to additional displacement.

The agreement of the present results showing a direct residual velocity dependence at small displacements (Figure 8) with the triaxial results of *Solberg and Byerlee* [1979], the smooth change from positive to negative B with displacement, and the dependence of B on surface

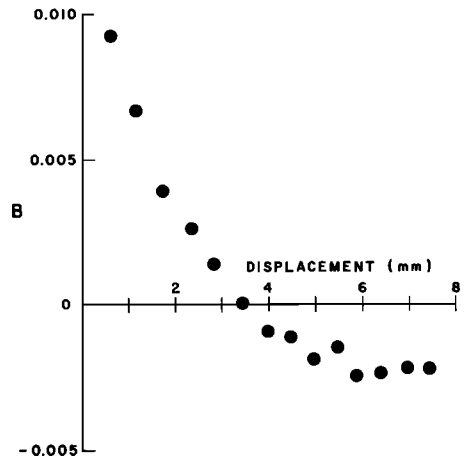

Fig. 8. B versus displacement for a test in which the velocity was cycled between 0.25, 2.5, and 25 μm/s from the beginning of the test. Note that the residual velocity dependence is initially positive and that it becomes negative with displacement. This experiment used 1 mm of gouge, <250 μm in contact with rough surfaces.

roughness (Figure 7) indicate that the different values of B seen in various experiments result from variations in the relative magnitudes of the two competing processes that alone give either positive or negative velocity dependence. Note, for example, that two tests in Figure 7 have $B = 0$. For those tests it is concluded that the process giving positive velocity dependence exactly offsets the process giving negative velocity dependence. The conclusion that competing velocity-dependent processes operate even when $B = 0$ is supported by the stress versus displacement records for those tests that show an initial but transient positive jump in μ when the velocity is increased followed by a decay to a zero net change of μ as the displacement increases. The point here is that the direct velocity effect is fully manifest immediately and causes the initial jump of μ. The competing velocity effect requires finite displacement to become fully evident and results in the progressive cancellation of the jump of μ as displacement increases. The final sign and magnitude of B reflect the magnitude of both velocity-dependent processes.

Recall from the earlier discussion of Figure 7 the conclusion that less negative values of B correlate with greater comminution of the gouge. This speculation is supported by the test illustrated by Figure 8, which displays positive values of B at the initial stages of slip where the rate of grain crushing is most likely a maximum. Later in the deformation, when B becomes negative and when shear zones are apparently well established, proportionately greater amounts of the deformation might take place by actual slip of particles past each other.

Figure 9 summarizes the relationship of the displacement required to reach the residual strength d_r to surface roughness, gouge thickness, and particle size. The variation of μ with displacement following a sudden velocity step was noted previously [*Dieterich*, 1978*a*, 1979*a*] and interpreted to be caused by a change in a velocity-dependent characteristic of the population of contacts between particles of gouge or across the slip surface. The two assumptions here are (1) there is some characteristic of the contacts that gives the inverse velocity dependence and (2) the displacement d_r required to reach a stable strength value following a velocity change is related to the displacement required to change completely the population of intergrain contacts established during slip at the previous velocity. A good correlation of d_r to surface roughness was found for the rock on rock tests supporting this conclusion [*Dieterich*, 1979*a*]. As shown by Figure 9, surface roughness and particle size both affect d_r in the present experiments. In addition, there is perhaps a weak indication that d_r may be larger for the thicker layers. The control of d_r by surface roughness and the weak or possibly nonexistent effect of thickness point again to the probable importance of concentrated shear zones that are strongly influenced by the roughness of the gouge-rock contact. The data in Figure 9 suggest that the coarser element of either the gouge or the surface roughness determines d_r. For example, with fine surfaces there are pronounced differences in d_r that appear to reflect the gouge particle size. For the rough surfaces the surface roughness is large in comparison to all but the coarsest particle sizes in the 125- to 250-μm gouge, and the d_r for the <85-μm gouge and the <250-μm gouge appear to be comparable.

Time Dependence

Time-dependent increase of the frictional strength of rocks has been observed in a variety of experiments and

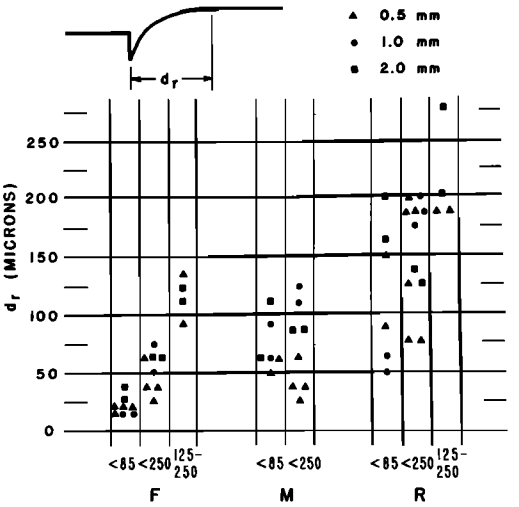

Fig. 9. Summary of the dispalcement d_r required to reach the residual strength following a factor of 10 change of velocity. Conditions for these measurements correspond to those of Figure 7. In addition, all measurements were made for decreases in velocity only. The upper curve shows an example of the stress versus displacement records from which the data were taken.

has been discussed at length in the literature [*Dieterich*, 1972; *Scholz et al.*, 1972; *Scholz and Engelder*, 1976; *Teufel and Logan*, 1978]. Time-dependent friction is related to observations of the residual velocity-dependent friction and directly underlies the causative mechanism of stick slip [*Dieterich*, 1978*a*]. The experimental curve of Figure 10 gives a stress versus displacement record that illustrates the characteristics of the time dependence tests. Note that the stress drops during the time the driving ram is held stationary (*a* to *b*). This is caused by slow continued slip of the surfaces at a rate that decays with time. Following the hold cycle the driving ram resumes motion at a constant velocity, and the gouge shows a transient increase in strength (*b* to *c*) that depends on the duration of the time that the ram was held stationary. Similar stress versus displacement records were found for the gouge-free tests reported by *Dieterich* [1979*a*]. The time-dependent increase in strength $\Delta\mu$ is taken to be defined by the stress maximum (level *c* minus level *a*). For all combinations of parameters with the present experiments, quantitatively similar increases in strength were observed when the driving ram was held stationary for a specific interval of time. The data of Figure 10 summarize the time dependence tests and give the peak increase of μ relative to the residual value of μ observed during slip at 2.5 μm/s that directly preceded and followed each hold cycle. Hold periods of 1, 10, 100, and 1000 s were used. The data appear to show a weak control of the time-dependent strength increase by the gouge particle size and the surface roughness. Within the scatter of the data, gouge layer thickness does not display a relationship to the magnitude of the time-dependent effect. The magnitude of the strength increases observed for the simulated gouge is within the range of values reported for nominally gouge-free surfaces [*Dieterich*, 1972].

A minimum displacement of 1.25 mm and a maximum of 6.0 mm were required to reach the large-scale residual strength preceding the hold cycles for the tests of Figure 10. A single exploratory experiment using 1 mm of gouge, <250 μm, and rough surfaces examined the effect of total displacement on the time dependence. This experiment (Figures 11*a* and 11*b*) employed 100-s hold cycles at successively greater displacements beginning at 0.25-mm total displacement. Sliding velocity between holds was 2.5 μm/s. Figure 11*a* gives the increase of strength, $\Delta\mu$, for the 100-s holds as a function of displacement. Figure 11*b* plots the displacement required to reach residual strength d_r following each hold cycle. The points P and R mark the approximate total displacements for the large-scale peak and residual strengths, respectively. There are two noteworthy features in Figure 11. First, the time-dependent effect becomes stable before completion of the large-scale displacement weakening and at relatively small total displacements (~1.75 mm) compared to the stabilization of the residual velocity effect in Figure 8 (5-6 mm). Second, d_r appears to decrease at the point where the large-scale displacement weakening effect is completed. The latter observations suggest that perhaps the deformation becomes fully localized at that displacement.

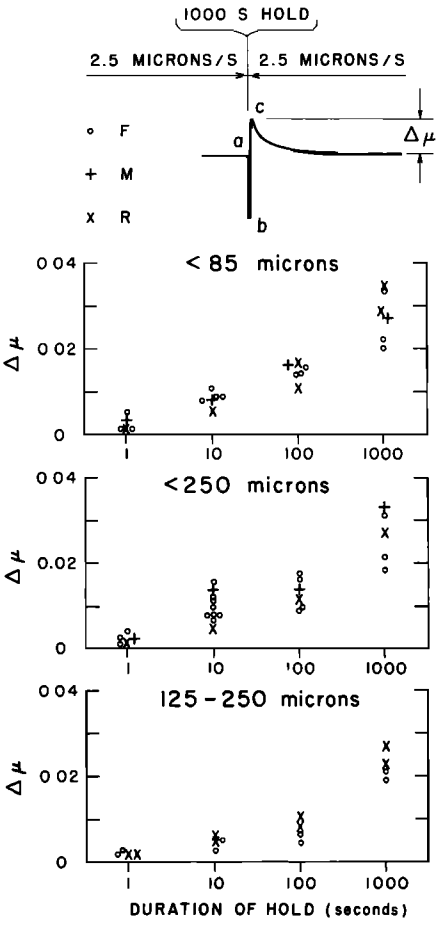

Fig. 10. Summary of observations of time-dependent increase of the strength following holds of 1, 10, 100, and 1000 s. The circles, pluses, and crosses refer to fine, medium, and rough surfaces, respectively.

Creep Test

Solberg et al. [1978] and *Solberg and Byerlee* [1979] report on a series of creep tests on simulated gouge consisting of crushed Westerly Granite in contact with intact Westerly Granite. Those experiments employed a triaxial testing apparatus and were conducted at confining pressures to 450 MPa. In those tests the axial load was raised in small increments and held constant at each increment for 12 hours. They found a strong dependence for the rate of deformation on time and stress level. At the lowest stress levels at which permanent deformation was seen, the deformation rate decayed with time in a manner resembling transient creep. At higher stress levels the initial transient creep phase gave way to approximately steady state or secondary creep. The creep rates increased with the stress level, indicating a direct velocity dependence of the gouge strength. At still higher stresses the

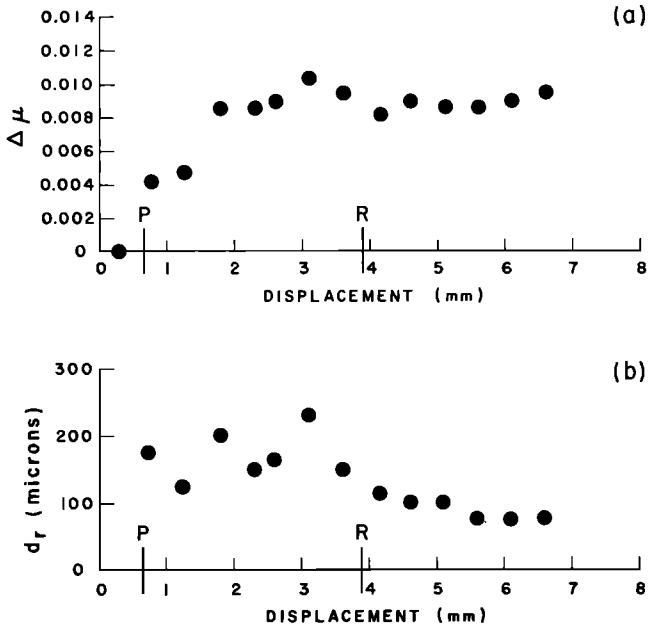

Fig. 11. (*a*) Time-dependent increase of μ for 100-s hold cycles as a function of displacement. (*b*) Displacement d_r required to erase the increase in strength caused by the hold cycle.

creep rate accelerated and instability resulted. These results clearly suggest a relationship to the usual types of creep behavior seen in solids. The positive velocity dependence indicated by the steady state creep results may at first consideration appear to contradict the inverse velocity dependence of the residual strength seen in this and previous studies.

In an attempt to clarify the relationship of the present experiments and the previous constitutive models to the higher-pressure creep measurements a few creep tests were run at 10-MPa normal stress. The specific purpose was to see if creep results similar to those obtained by *Solberg et al.* [1978] could be obtained, and if so to establish the connection of the creep measurements to the constitutive model proposed by *Dieterich* [1979*a*]. The experiments employed the <250-μm gouge in 1-mm layers in contact with a rough ground surface. Figure 12 plots the displacement against time for a creep experiment within which the gouge layer has not been preconditioned with slip. Although the present experiment was not carried to such long time intervals as those of Solberg et al., the results of Figure 12 look very much like the effects reported by Solberg et al., and it is concluded that similar processes are active in each experiment. Because the displacements of the block are small throughout this experiment, the results from Figure 8 indicate that the residual velocity effect should show a positive dependence on velocity. Hence except for the difference in normal stress and duration of the test, the experimental conditions and results appear to be fully compatible with those of *Solberg et al.* [1978].

A second test was run using the same fault parameters, but the gouge layer was first preconditioned by 5.5 mm of slip to determine the effect of negative residual velocity dependence on the creep results. From Figure 8, recall that the initial positive velocity dependence becomes negative following a few millimeters of displacement. For this creep test following the preconditioning the shear stress was not set to zero but was lowered to the first hold stress of 5.64 MPa. Figure 13 gives the results of the test. Although creep is observed over a small range of shear stresses and the total displacements are much less than those observed for the test without preconditioning, the general character of the results is similar to the results of Figure 12. It would appear therefore that the creep type of behavior observed in these experiments and the high-pressure triaxial results is enhanced by a positive residual velocity dependence but that it does not require it. Below it will be shown that the creep is made possible by the mechanism that causes the jump of strength seen for the transient velocity effect.

Constitutive Model

In a qualitative sense most of the experimental data described above agree with the results obtained previously

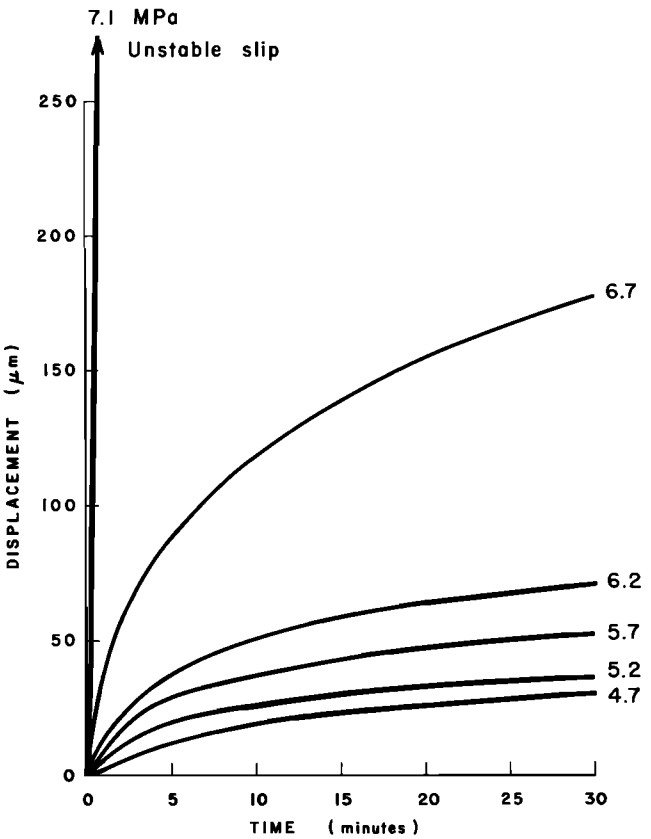

Fig. 12. Displacement versus time for a creep test with 1.0 mm of <250-μm gouge in contact with a rough surface. This gouge layer was not preconditioned by prior slip. Labels on the curves give the value of the shear stress in megapascals.

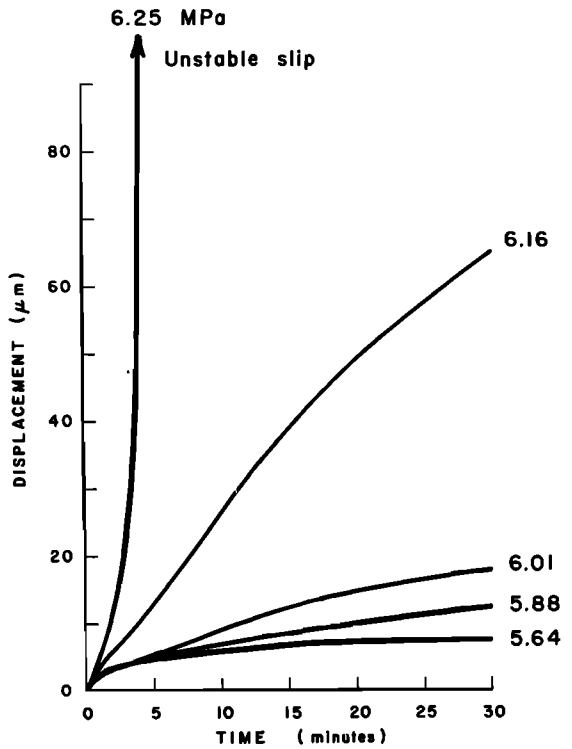

Fig. 13. Displacement versus time for a creep test with 1.0 mm of <250-μm gouge in contact with a rough surface. This gouge layer was preconditioned by 3.0 mm of slip. Note change of scale for displacements compared to Figure 11. Labels on the curves give shear stress in megapascals.

for nominally gouge-free surfaces of granite. In particular, following preconditioning, the overall form of the stress-displacement curves, the time dependence, the transient velocity effect, and the residual velocity effect are very similar to those observed previously. The magnitude of d_r is significantly greater for gouge than it is for gouge-free surfaces. The initial large-scale peak in the stress-displacement curves was not observed in the prior friction experiments and does not seem to be explainable by the fault friction constitutive model in its present state. The observations here and those of *Tchalenko* [1970] and *Logan* [1979] indicate that the large-scale displacement weakening from the peak strength at the beginning of a run is associated with the localization of the deformation into distinct shear zones. This probably results in a change in the dominant mode of deformation from breaking of interlocked grains throughout the gouge layer to localized deformation consisting more nearly of slip on surfaces within the gouge or at the gouge-rock contact. The large magnitude of the displacement required to reach stabilization at a residual strength and the sensitivity of the velocity-dependent parameter B to initial displacements may present problems for interpretation of experimental results in which the total displacements are limited. Because the peak appears to become reestablished only following a large stress drop, the large-scale displacement weakening may not be important for natural faults if stress changes are small, i.e., small stress drops in earthquakes. At any rate, the large-scale stress maximum and possible localization effects are not considered in the following discussion.

The following discussion of constitutive relations is based on the constitutive model previously outlined by *Dieterich* [1979*a*]. The basis of that model is that the coefficient of friction μ can be expressed as the product

$$\mu = CF \tag{2}$$

where C is proportional to the strength of the load-bearing asperities in response to the applied normal stress and F is inversely proportional to the strength of the asperities in response to the applied shear stress. Note that CF is dimensionless and independent of normal stress. The central notion of the model is that F, the strength of the asperities in shear, is a direct function of slip velocity and that C, which controls the size of the asperities, is a function of a history-dependent parameter θ. Several lines of evidence suggest that θ is the effective age of the asperities and that the observed time-dependent increase of fault strength occurs because the area of contact of the asperities increases with time [*Dieterich*, 1978*a*]. A specific empirical relationship for C that satisfactorily accounts for the increase in μ with time is

$$C = c_1 + c_2 \log_{10} (c_3\theta + 1) \tag{3}$$

The parameters c_1, c_2, and c_3 are constants, and θ is proportional to the average age in seconds of the asperities. The dimensions of c_3 are s^{-1}. The mechanism for the increase in the size of the asperities is interpreted to be asperity creep in response to the normal stress [*Dieterich*, 1972, 1978*a*; *Scholz and Engelder*, 1976]. The observation of the transient velocity dependence (i.e., the jump in strength that occurs when velocity is suddenly changed) was interpreted to be evidence for a velocity dependence of the shear strength. The following empirical relationship was proposed by *Dieterich* [1979*a*, *b*]:

$$F = f_1 + \frac{1}{f_2 \log_{10} (f_3/V + 10)} \tag{4}$$

where f_1, f_2, and f_3 are constants and V is the slip velocity. Note that (3) and (4) imply a similar type of time dependence of strength of the asperities that is consistent with the usual behavior of rock-forming minerals. The parameter f_3 has dimensions of microns per second. The specific form for (4) is as yet poorly defined, and it appears that a number of similar empirical relationships fit the data equally well. The following relationship for F agrees with the observations as well as (4) and has the slight advantage of making the relationship of C to F somewhat more transparent:

$$F = \frac{1}{f_1 + f_2 \log_{10} (f_3/V + 1)} \tag{5}$$

The constants f_1, f_2, and f_3 do not have the same numerical values as (4). Note that the form of (5) is the inverse of (3) if f_3 has the dimensions of velocity. Equation (5) is used in preference to (4) for the remainder of this paper.

Because of fault displacement, the load-bearing contacts across the fault or between particles of gouge in the fault are continuously created and destroyed at a rate that is proportional to the rate of slip. For steady state slip at a constant velocity the average age of the contacts is

$$\theta = d_c/V \tag{6}$$

where d_c is proportional to the displacement required to change an existing population of asperities completely. The use of (6) in (3) along with (5) gives the steady state or residual strength as a function of velocity. Because a finite displacement proportional to d_c is required to change the contacts, a change of velocity does not result in an immediate change of θ. In order to use these relationships for computations to follow the change in strength following a change in velocity, it is necessary to follow the resulting change of θ with displacement. *Dieterich* [1979*a*, *b*] proposed the following function to follow the evolution of θ with displacement d for a step change to velocity V at displacement d:

$$\theta = (d_c/V) * (\theta_0 V/d_c)^{\exp[(d_0-d_c)/d_c]} \tag{7}$$

The time of contact at d_0 is θ_0. Note that as d increases from d_0 to $d \gg d_0$, θ goes from θ_0 to d_c/V. Detailed simulations of experiments in which the velocity changes continuously with displacement are possible using (7) by breaking the velocity into small constant velocity steps [*Dieterich*, 1979*a*, *b*]. Recently, *Rice* [1981], A. Ruina (unpublished manuscript, 1980), and *Kosloff and Liu* [1980] have investigated differential formulations based on (7) or similar functions that permit continuously varying velocity histories to be more accurately represented. A. Ruina (personal communication, 1980) has pointed out a potential problem with (7) that can arise for sudden decreases in velocity. As V goes to zero, $d\theta/dt$ also goes to zero. This is undesirable if the original concept that θ increases with time for stationary surfaces is correct. For the following equation, which is based on one proposed by Ruina, $d\theta/dt$ goes to 1 as V approaches zero:

$$\theta = (d_c/V) + (\theta_0 - d_c/V) \exp\left(\frac{d_0 - d}{d_c}\right) \tag{8}$$

The observations of time, velocity, and displacement dependence described above agree with the previous observations for friction of gouge-free surfaces [*Dieterich*, 1979*a*] and give added support for the validity of the general form of the model. Those observations have been used to derive specific values for the parameters in (3), (5), and (6) for the various combinations of experimental variables. The values are given in Table 1. Because the magnitudes of the time and velocity effects are small in comparison to the magnitude of the total strength of the gouge, the approximate magnitude of μ for the fault is controlled by the relative values of c_1 and f_1. By arbitrarily setting the value of f_1 at 1.0, c_1 is then approximately the value of the μ in the absence of the time and velocity effects. In general the results summarized in Figures 7, 9, and 10 indicate that d_c and the time and velocity dependence are insensitive to gouge layer thickness. Consequently, the data for different layer thicknesses have been lumped within a single category for particle size and surface roughness. Note that parameter c_3 controls the lower limit that time-dependent effects can be seen and that f_3 similarly controls the maximum velocity for which velocity-dependent effects are seen. Because the present experiments were over a limited range of times and velocities, c_3 and f_3 are undefined, and the values given in Table 1 represent the approximate lower limits permitted by the observations. To obtain a fit of the data for c_2, it is necessary to know the value of d_c because the value of θ after a hold period is approximately the sum of the age of the contacts during the slip that immediately preceded the hold, θ_0, and the hold time, θ_h:

$$\theta = \theta_0 + \theta_h \tag{9}$$

where from (6),

$$\theta_0 = d_c/V \tag{10}$$

The values of d_c in Table 1 are those that were used to obtain c_2 and give the best fit of the time-dependent data using the numerical model described in the following section.

From (3), (5), and (6) for steady state slip at a constant velocity V (i.e., the displacement velocity at V is greater than d_c),

$$\mu = \frac{c_1 + c_2 \log_{10}(c_3 d_c/V + 1)}{f_1 + f_2 \log_{10}(f_3/V + 1)} \tag{11}$$

Hence parameter c_2, which controls the time dependence, also gives the inverse velocity-dependent effect. Parameter f_2 controls the direct velocity effect. The total residual velocity dependence B in Figure 7, observed when comparing the steady state values for μ at different velocities, is determined by both c_2 and f_2. In Table 1, note that c_2 shows a weak but systematic correlation with surface roughness and that f_2 shows a stronger correlation with surface roughness. As a result of those variations with roughness it is possible to identify which of the competing velocity effects is most important in controlling the observed variations of B with surface roughness. Table 1 shows that the inverse velocity effect is slightly enhanced by increasing the roughness of the surfaces (tends to decrease B slightly) and the direct velocity effect is greatly enhanced for the rough surfaces (tends to increase B greatly). The observed higher values for B for rough surfaces therefore are caused by enhancement of the direct velocity effect as suggested by the earlier observations on comminution and not by a weakening of the process con-

TABLE 1. Constitutive Parameters

Gouge Size, μm	Roughness	d_r, μm	d_c, μm	c_1	c_2	c_3, s^{-1}	f_1	f_2	f_3, μm/s
125-250	R	225	50	0.60	0.017	>0.5	1.0	0.025	>25
125-250	F	115	25	0.50	0.014	>1.0	1.0	0.012	>25
<250	R	140	37	0.63	0.019	>0.07	1.0	0.027	>25
<250	M	65	12	0.60	0.019	>2.0	1.0	0.023	>25
<250	F	50	7	0.57	0.019	>3.6	1.0	0.021	>25
<85	R	125	37	0.65	0.020	>0.07	1.0	0.027	>25
<85	M	75	17	0.64	0.019	>1.5	1.0	0.022	>25
<85	F	20	4	0.61	0.017	>6.3	1.0	0.018	>25

trolling the inverse effect. Figure 10 supports a similar conclusion for the variation of B with displacement illustrated in Figure 8. In Figure 10 the magnitude of the time dependence and hence c_2 do not change for displacements to 5–6 mm.

Numerical Model for Fault Interactions

It was noted above that this study was done from the perspective that slip phenomena observed for simulated faults and for natural active faults arise from the combined effects of the constitutive properties of the fault and the total mechanical system that loads the fault. Attempts to understand the observations without accounting for these interactions can be seriously incomplete. To simulate the specific experimental results of this study and to explore some of the implications of the interactions between the constitutive properties of a fault, a simple deterministic numerical model has been developed. The analysis is based on a zero-mass slider and spring system (Figure 14). The spring with stiffness K represents the combined elastic properties of the system that interacts with the fault. At this point it should be noted that it is surely an understatement to say that this model is a simple idealization of laboratory or natural faulting. Natural faults, especially, certainly involve three-dimensional interactions in which heterogeneity of properties on the fault and geometric deviations from perfectly planar fault surfaces probably have fundamental importance. However, previous investigations [*Dieterich*, 1978*a*, 1979*a*] indicate that the slider-spring model is sufficient to explore some of the first-order interactions that underly the different slip modes. The model presented here is intended to illustrate some of those interactions in more detail and to provide a detailed check of the applicability of the constitutive model to simulated gouge.

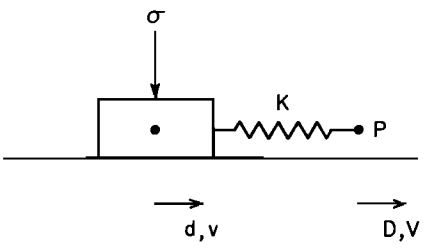

Fig. 14. Spring and slider model.

With this model the slider is externally loaded by specifying the displacement D, velocity V, or loads at the loading point P (Figure 14). For simulation of the present experiments the motion of the loading point P corresponds to the observed displacements because those displacements were controlled by the servo control system. Displacement and velocity of the slider are d and v, respectively. The area of the slider is unity. Normal stress is applied to the block independent of the conditions at the loading point. Shear stress τ is specified by the deformation of the spring:

$$\tau = K(D - d) \tag{12}$$

For the purposes of the computations it is convenient to nondimensionalize the equations for displacements and stresses. Below, the normalized quantities are indicated by primed symbols. Terms containing displacements are divided by the critical displacement d_c, and terms containing stress are divided by σ:

$$D' = D/d_c \tag{13}$$

$$V' = V/d_c \tag{14}$$

$$d' = d/d_c \tag{15}$$

$$v' = v/d_c \tag{16}$$

$$\tau' = \tau/\sigma = \mu \tag{17}$$

$$K' = (K)\,(d_c/\sigma) \tag{18}$$

Note that shear stress τ reduces to μ and that changes in the normalized stiffness of the spring can be brought about by changes in σ, d_c, or K.

The computational procedure employed for this model is deterministic and uses a displacement marching scheme in which the slider velocity v is assumed to be constant during each step. Displacement steps are generally $d_c/20$. For each displacement step the principal unknown of the computation is the slider velocity. An iterative procedure is employed to find v such that the friction force at the end of the step equals the spring force. At the beginning of

each displacement step a trial slip velocity v is used to define the duration T of the step:

$$T = d_c/(20v)$$

Using T the displacement at the loading point appropriate to the specified loading history is set. The evolution of θ is then calculated from (7) or (8), and the friction force is found from v and θ. If the absolute difference between μ and $(K)(d - D)$ is greater than 10^{-6}, then a correction is added to the trial velocity, and the procedure is repeated until μ and the spring force are equal. When v is determined, the displacement is then incremented, and the iteration for the next step is begun.

The computational procedure is modified slightly for simulation of the time dependence and creep tests where the velocity may become very small and consequently T becomes very large. In those situations the computer program reduces the displacement step from $d_c/20$ to a suitably small value such that the time required for a displacement step does not exceed the time required for a specified change in the applied loading conditions (for example, resumed action of the loading point following a hold period).

A slip instability can arise with this model if the decrease in μ with displacement exceeds the slope of the unloading curve which is fixed by K'. As a slip instability is approached, the system responds by increasing the slider velocity such that the direct velocity term in (5) is sufficient to keep the friction force in balance with the spring force. Because of the higher velocity, θ decreases with displacement, and to maintain equilibrium, a higher v is required for the next displacement step, and so on. However, as $v \gg f_3$, further velocity increases no longer directly affect μ, and the evolution of θ alone controls the change of μ with displacement. This causes μ to decrease rapidly with displacement. In this case the applied load exceeds the frictional resistance, and the assumption of quasi-static equilibrium employed for the computations is violated. During high-velocity slip, changes of μ are controlled initially by the decrease of θ with displacement. For the case $\theta \ll 1/c_3$, μ is insensitive to θ. A procedure that permits unstable slip in the present model is to assume an upper limit for the slider velocity of $v = 100f_3$, since higher velocities do not contribute to the direct velocity dependence. During the computations, if v exceeds $100f_3$, an instability will occur because μ will drop suddenly independent of v. When this occurs, the slider velocity is fixed at $100f_3$, and computations for μ proceed independent of the assumption of equilibrium. This assumption of instability continues until the displacement of the slider is sufficient to reduce the spring force to equal the frictional strength, whereupon the assumption of quasi-static equilibrium is reasserted. Clearly, a number of simple refinements could be added to this procedure to represent better the conditions during an instability. The purpose of the present procedure is not to follow the detail of interactions during an instability but to allow the computations to continue through the instability without becoming trapped by a numerical condition that could not satisfy the assumptions of quasi-static equilibrium.

Simulation of Slip Modes

Figure 15 gives three examples of simulations using different stiffnesses K' that illustrate some features of the computations and show the details of the onset of a stick slip instability following a hold period of 100 s. Parameters for the constitutive law are $d_c = 20$ μm, $c_1 = 0.60$, $c_2 = 0.014$, $c_3 = 1.0$, $f_1 = 1.0$, $f_2 = 0.014$, and $f_3 = 1.0$. Effective stiffnesses are 0.01250, 0.00236, and 0.00125 for Figures 15*a*, 15*b*, and 15*c*, respectively. The motion of the loading point is initially 2.5 μm/s (points 1-2, Figure 15), followed by a 100-s hold (2-3), followed by resumed motion at 2.5 μm/s. The evolution function for θ given by (7) was used for each simulation. For the case in Figure 15*a*, sliding is stable at all times. Note the overall similarity of the stress versus displacement record for Figure 15*a* with that observed experimentally (Figure 10), including the stress relaxation due to slip during the hold interval. The increase in strength arises because θ increases during the hold when the slider moves at progressively slower velocity. The finite slope of the stress drop during the hold cycle of each simulation (2-3 in Figure 15) differs from the vertical slope of the experimental record. This difference results solely from the fact that the simulations show the motion of the block while the experiments give the motion of the loading point. The slopes of the stress drop equal the stiffness K'. The continued motion of the slider after the loading point is held stationary is a consequence of the direct velocity term in the constitutive law and finite stiffness of the spring. Additional slip results in a decrease in

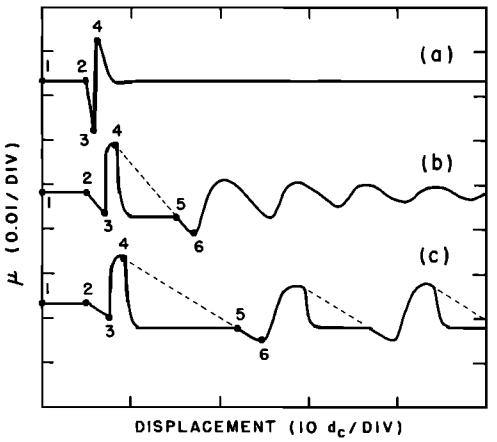

Fig. 15. Simulations showing the effect of stiffness K' on a test in which the loading point is held stationary for 100 s. The dashed line shows the spring force acting on the slider during an unstable slip event. Stiffnesses are 0.0125, 0.00236, and 0.00125 for Figures 15*a*, 15*b*, and 15*c*, respectively.

stress with displacement that has a slope determined by K'. As a consequence of the direct velocity term F, slip can occur at reduced stress if v is sufficiently reduced also. This slip of the block decays with time and results in a relaxation of the stress. The rate of stress relaxation is controlled by the rate of slip and the stiffness of the spring.

For intermediate and low stiffnesses (Figures 15*b* and 15*c*), unstable slip follows the resumption of loading because the transient increase of μ caused by the hold cycle decays with displacement at a rate that exceeds K'. The dashed line (points 4-5) gives the stress acting on the slider by the spring and has a slope of $(-K')\,(1 - V/100f_3)$. The solid line gives the fault strength. The imbalance of spring and frictional stress provides the driving force for the slip instability. It is important to point out that to maintain equilibrium, slider velocity increased from $v \ll 2.5$ μm/s at point 3 to $v = 100$ μm/s at point 4 in Figures 15*b* and 15*c*. This type of accelerating preinstability slip is a common feature of laboratory stick slip [*Byerlee*, 1967; *Logan et al.*, 1972; *Scholz et al.*, 1972; *Dieterich*, 1978*b*]. Between points 4 and 5 in Figure 15 there is no slider velocity that permits quasi-static equilibrium. At point 5 the displacement of the slider is sufficient to reduce the stress applied to the slider by the spring to the fault strength, and the equilibrium condition is again asserted for the computations. The continued stress drop from points 5 to 6 results from interactions that are similar to the stress drop during the hold cycle. At point 5 the slider velocity is $100f_3$ (100 μm/s), and at point 6 the slider velocity and velocity of the loading point are equal (2.5 μm/s). Because of the direct velocity-dependent term, the deceleration of the slider results in a decrease of the frictional strength, which is followed by the spring.

For the simulations of Figure 15, note that for intermediate K' the slip instability is followed by stable but oscillating slip and the low-K' example has repeated unstable slip (stick slip). This change in slip mode for change in K' corresponds directly to the experimental observations of *Dieterich* [1978*a*] that show the transition from stable to unstable slip occurs when σ is increased, machine stiffness is decreased, or d_c is decreased. Recall from (18) that K' is similarly dependent upon K, σ, and d_c. For the simulations, oscillatory slip occurs only for a narrow range of values of K' near the transition from constant velocity stable slip and stick slip. This corresponds to the experimental observations of oscillatory slip near the transition from stable to unstable slip by *Scholz et al.* [1972].

Simulation of Time Dependence Tests

Figure 16 shows simulations of a time-dependent test that illustrate some of the characteristics of the two evolution functions (7) and (8). Figure 16*a* gives the experimental results for 1 mm of gouge, <250 μm in contact with rough surfaces. The simulation shown by Figure 16*b* uses (7) and has an overall form that resembles the experimental data, but the magnitudes of the peak strength following the hold are less than the magnitude observed in the

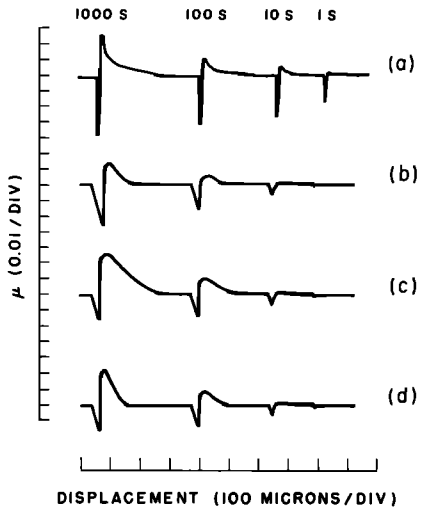

Fig. 16. (*a*) Experimental results of a time dependence test using 1 mm of gouge, <250 μm in contact with rough surfaces. (*b*, *c*, *d*) Simulations with $c_1 = 0.63$, $c_2 = 0.019$, $c_3 = 1.0$ s^{-1} and $f_1 = 1.0$, $f_2 = 0.027$, $f_3 = 1.0$ μm/s.

experiments. That is because of the characteristic noted above that $d\theta/dt$ goes to zero as the velocity of slip goes to zero. As a result, θ at the end of the hold cycle is too small, resulting in a lower peak when loading velocity is reapplied. Figure 16*c* is an identical simulation that uses evolution equation (8) instead. In the case of Figure 16*c* the height of the peaks agrees with the observations. The decay of strength following peak strength for Figure 16*c* is much slower than that for Figure 16*b*. This is because the change of θ with displacement for $\theta > (d_c/v)$ using (8) is not as rapid as (7). Figure 16*d* employed a composite of (7) and (8) to compute the evolution of θ. In the case of Figure 16*d*, (7) was used for $\theta > (d_c/v)$ and (8) was used for $\theta < (d_c/v)$.

Velocity Simulations

Figure 17 gives a comparison of the simulated multiple-velocity tests with the experimental stress versus displacement curves. The example is for gouge of <85 μm, 2 mm thick, and in contact with a rough surface. The constitutive parameters used are those given in Table 1.

For Figure 17, as in the case of the simulations of the time-dependent tests of Figure 16, the curves in Figures 17*b*, 17*c*, and 17*d* use evolution equation (7), evolution equation (8), and the composite of (7) and (8), respectively. The simulations of the velocity tests in Figure 16, unlike those of Figure 15, show little sensitivity to choice of the evolution equation.

Figures 18 and 19 give experimental curves and simulations for the multiple-velocity tests using <85-μm gouge, 2 mm thick, in contact with M and F surfaces, respectively (i.e., Figures 15, 16, 17 give the series of velocity tests with only surface roughness varying between tests). The

results using evolution equation (7) are shown. The other evolution models for θ give essentially similar results.

Simulation of Creep Tests

Figure 20 gives the results of a simulation of a constant stress creep experiment. Shear stress τ was held constant for an interval of 30 min and then increased to a higher level and held constant again for 30 min, and so on until a slip instability occurred. The initial value for θ was arbitrarily set at 10 s. The simulation attempts to approximate the conditions of Figure 12, which did not have an episode of slip preconditioning. The experiment used gouge of <250 μm in contact with rough surfaces giving d_c = 37 from Table 1. Because the gouge layer did not experience slip preconditioning, the data of Figure 8 indicate that B, the parameter for residual velocity dependence, had a positive value of approximately 0.009. Accordingly, constitutive parameters of $c_1 = 0.63$, $c_2 = 0.019$, $c_3 = 1.0$ s and $f_1 = 1.0$, $f_2 = 0.044$, $f_3 = 1.0$ μm/s were chosen for the model to give $B = 0.009$. In the absence of preconditioning, the results of this study show that velocity dependence, time dependence, and the gross strength level for constant velocity slip all change rapidly as a function of displacement in the early stages of a test. This simulation assumes all constitutive parameters to be independent of total displacement, and it is therefore only a rough approximation to the probable experimental conditions. It does, however, show the same general features as Figure 12. Creep with displacement rates that decay with time occurs at the lower stress levels. Because the stress and hence V are less than that required for steady state slip, $\theta > d_c/V$. This results in an increase of θ with time. That increase of θ tends to strengthen the gouge for constant velocity slip, but the direct velocity term F in the constitutive law permits the strength to remain constant if V decreases. The rate of velocity decrease in the simulations is less than that for

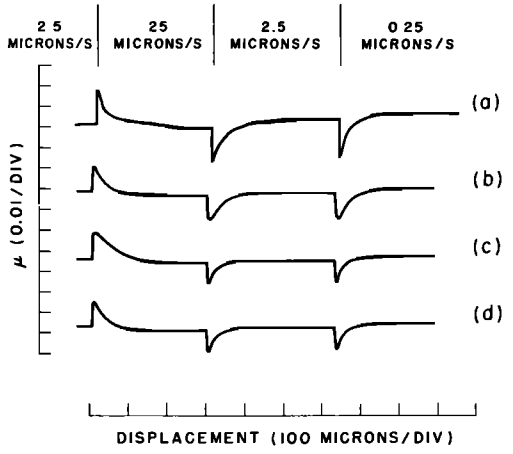

Fig. 17. Comparison of (*a*) experiment and (*b*, *c*, *d*) simulations for a multiple-velocity test with 2 mm of gouge, <85 μm in contact with rough surfaces.

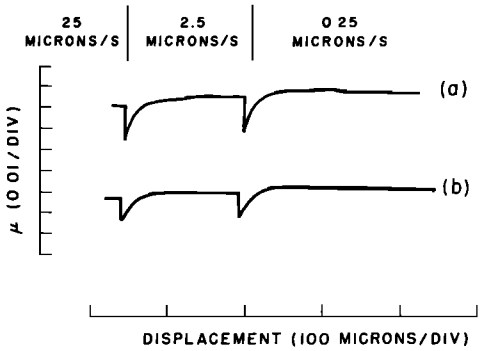

Fig. 18. Comparison of (*a*) experiment and (*b*) simulation for a multiple-velocity test with 2 mm of gouge, <85 μm in contact with medium surfaces.

the experiments, indicating that the evolution function for θ needs some refining. Total displacement for a 30-min constant stress interval and hence the average rate of slip increase with the applied shear stress. At the highest stress levels in the simulations and experiment, creep rapidly accelerates to unstable failure. Accelerating slip occurs because the stress increments eventually result in a slip velocity such that $\theta < d_c/V$. As a result, V must accelerate to keep the stress constant.

The simulation of Figure 21 corresponds approximately to the creep experiment of Figure 13. For that experiment the gouge had been fully preconditioned by an initial episode of constant velocity slip. Therefore constitutive parameters for this simulation were taken directly from Table 1 for the case of gouge of <250 μm in contact with rough surfaces. The constitutive parameters for the present model are identical to those of the previous model except that $f_2 = 0.044$ for the former and $f_2 = 0.27$ for the latter. Because of the preconditioning, the data of Figure 7 and indirectly the parameters from Table 1 indicate that the strength of gouge at steady state sliding is an inverse function of velocity. An interesting feature of the experiment and simulation is that the average velocities during the constant stress holds in the absence of other information would lead to the incorrect conclusion that gouge strength is a direct and not an inverse function of velocity. Note also that the results of Figure 21 compared to Figure 20 show that the effect of reducing f_2 from 0.044 to 0.027 is to reduce the amount of creep.

Discussion

These experiments display time-, velocity-, and displacement-dependent effects that qualitatively resemble effects reported previously for rock friction on initially clean surfaces [*Dieterich*, 1979*a*]. In addition, the constant stress creep experiments at successively higher stresses give results that appear to correlate with the high-pressure creep in simulated gouge reported by *Solberg et al.* [1978].

Following a change of velocity the displacement re-

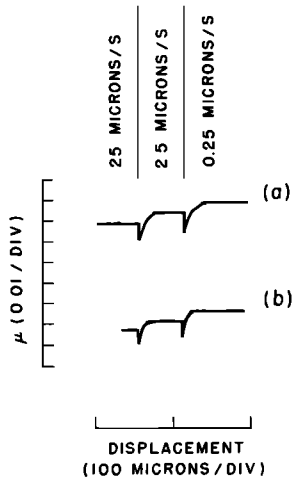

Fig. 19. Comparison of (*a*) experiment and (*b*) simulation for a multiple-velocity test with 2 mm of gouge, <85 μm in contact with a fine surface.

quired to reach a stable strength level d_r appears to reflect the displacement needed to change the population of intergrain contacts that govern the strength of the gouge. The parameter d_r is much larger for the gouge than it is for friction of surfaces free of gouge. Gouge particle size and roughness of the surface in contact with the gouge, but not the thickness of the gouge layer, control the magnitude of d_r. This result indicates that the deformation in the gouge is highly localized, probably at the gouge/rock contact. This conclusion is supported by previous studies of deformation structures from laboratory experiments [*Byerlee et al.*, 1978; *Logan*, 1979]. The observed time dependence, velocity dependence, and related displacement-weakening properties of the gouge probably contribute to the localization process. Because increase of the age of the contacts, θ, tends to strengthen the gouge, perturbations of the deformation rate within the gouge will tend to grow. Zones that deform at relatively slower rates will on the average have interparticle contacts that are older than more rapidly deforming zones. As a result of the greater contact times, the more slowly deforming zones will become stronger and the more rapidly deforming zones will become weaker, resulting in greater concentration of the deformation in the weakening zone.

These experiments and the previous experiments of *Dieterich* [1979*a*] give clear evidence for two competing velocity-dependent processes. Because one process responds immediately to velocity changes and the other requires a finite displacement d_r to become fully effective, the two processes become separable when the sliding velocity is suddenly changed to a new value. The immediate process acts to give a direct dependence between strength and velocity. Hence increases in velocity of slip are marked by an immediate increase in strength. The process that requires displacement d_r to become fully effective produces an inverse dependence of strength on velocity. As a result of the competition of the two processes, an increase of velocity first causes an increase in strength followed by a decrease of strength with displacement. The final residual change in strength caused by a change of slip velocity may be either positive or negative depending upon the relative magnitudes of the two processes. Both positive and negative changes are seen for gouge. The results of these tests

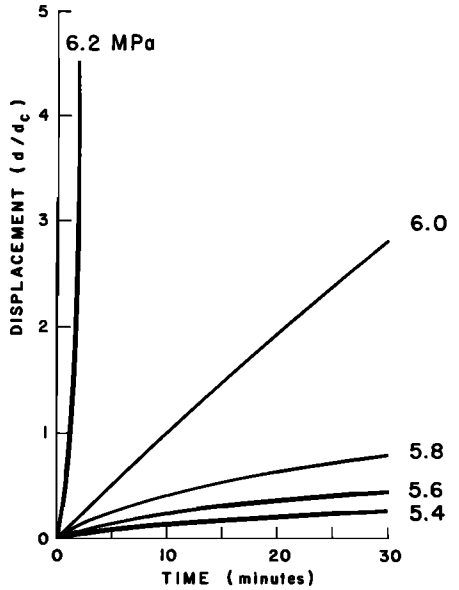

Fig. 20. Simulation of a creep test in which the constitutive parameters give the strength to be a positive function of steady state velocity ($B = 0.009$).

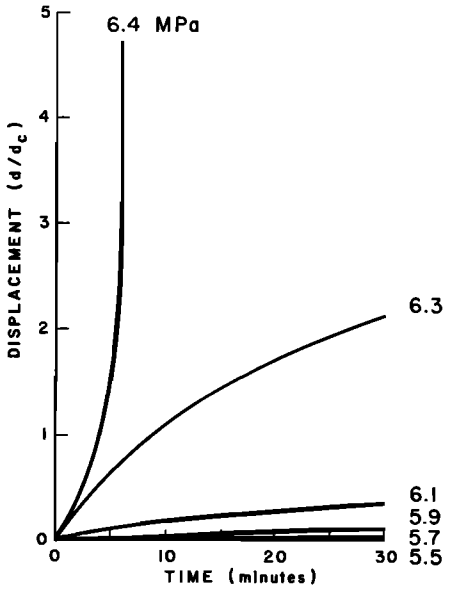

Fig. 21. Simulation of a creep test in which the constitutive parameters require the strength to be a negative function of steady state velocity ($B = -0.003$).

indicate that the process giving the negative effect is related to the time dependence and that it is relatively insensitive to experimental conditions. Experimental conditions more strongly influence the process giving direct positive velocity dependence. Apparently, the rate of comminution of the gouge directly affects the direct dependence on velocity. The magnitude of the direct velocity-dependent process and the strength of the gouge are greater for conditions that lead to maximum rates of comminution.

Numerical computations using the constitutive model with a simple spring and slider are in good agreement with the various experimental observations reported here. The significant aspect of the simulations is not that a single result can be reproduced in detail but that the model is capable of representing the full range of experimental effects. The results of simulations of the multiple-velocity tests are largely insensitive to the choice of evolution law for θ. Simulations of the time dependence tests all have the same general form as the experimental results, but there are some differences in the peak strength and decay of the peak with displacement that indicate further refinements in the evolution equations for θ may be required. An interesting aspect of the experiments and simulations of the time-dependent tests is that during the hold cycle, when the loading point is held stationary, the slider continues to move at rates that decay with time. This motion has the same underlying mechanism as that causing creep of the gouge at constant stresses. It arises because of the direct velocity term in the constitutive law and the finite stiffness of the system. In a system with infinite stiffness any motion of the slider would cause the stress to drop to zero. Hence continued slip would not be possible. Model and experimental creep tests show similar features. A specific result of the creep experiments and simulations is that although both the competing direct and inverse velocity-dependent processes operate during the deformation, the results taken alone could be erroneously interpreted to be evidence for only a direct, positive dependence on velocity. However, if an interpretation is adopted that only a positive dependence on velocity exists, then the acceleration of slip to an instability at the highest stress is unaccounted for, because instability requires some form of weakening with displacement.

Finally, the model is able to reproduce different modes of sliding including stable slip, oscillatory slip, and unstable slip by varying the stiffness of the system that loads the fault, the normal stress, or the gouge/surface property measured by d_c. Accelerating slip always precedes the onset of unstable slip. At the beginning of this report it was pointed out that these modes of slip are analogous to modes of slip seen for active faulting. In addition, the observation of earthquake afterslip, which shows a decay of the rate of slip with time, may be equivalent to the slip seen during the hold periods of the time tests and the decelerating slip of the creep tests. If this interpretation is correct, then the mechanism allowing afterslip might involve the following: During earthquake slip the velocity is high, and therefore θ, the average age of the stress bearing contacts in the slip zone, will be small. Because of the direct velocity effect, slip may continue at a reduced stress following an earthquake if the sliding velocity is low. At the lower velocity of slip the average age of the contacts will increase, resulting in a strengthening of the fault gouge and a further slowing of the afterslip.

References

Byerlee, J. D., Frictional characteristics of granite under high confining pressure, *J. Geophys. Res.*, *72*, 3639-3648, 1967.

Byerlee, J., and R. Summers, A note on the effect of fault gouge thickness on fault stability, *Int. J. Rock Mech. Mining Sci. Geomech. Abstr.*, *13*, 35-36, 1976.

Byerlee, J., V. Mjachkin, R. Summers, and D. Voevoda, Structures developed in fault gouge during stable sliding and stick-slip, *Tectonophysics*, *44*, 161, 1978.

Dengo, C. A., and J. M. Logan, Correlation of fracture patterns in natural and experimental shear zones (abstract), *Eos Trans. AGU*, *60*, 955, 1979.

Dieterich, J. H., Time-dependent friction in rocks, *J. Geophys. Res.*, *77*, 3690-3697, 1972.

Dieterich, J. H., Time-dependent friction and the mechanics of stick-slip, *Pure Appl. Geophys.*, *116*, 790-806, 1978*a*.

Dieterich, J. H., Preseismic fault slip and earthquake prediction, *J. Geophys. Res.*, *83*, 3940-3948, 1978*b*.

Dieterich, J. H., Modeling of rock friction, 1, Experimental results and constitutive equations, *J. Geophys. Res.*, *84*, 2161-2168, 1979*a*.

Dieterich, J. H., Modeling of rock friction, 2, Simulation of preseismic slip, *J. Geophys. Res.*, *84*, 2169-2175, 1979*b*.

Engelder, J. T., J. M. Logan, and J. Handin, The sliding characteristics of sandstone on quartz fault-gouge, *Pure Appl. Geophys.*, *113*, 69-86, 1975.

Kosloff, D. D., and H.-P. Liu, Reformulation and discussion of mechanical behavior of the velocity-dependent friction law proposed by Dieterich, *Geophys. Res. Lett.*, *7*, 913-916, 1980.

Logan, J. M., Laboratory and field investigations of fault gouge, contract report, grant No. 14-08-0001-17677, 89 pp., U.S. Geol. Surv., Menlo Park, Calif., 1979.

Logan, J. M., T. Iwasaki, M. Friedman, and S. Kling, Experimental investigation of sliding friction in multilithologic specimens, *Eng. Geol. Case Hist.*, *9*, 55-67, 1972.

Rice, J. R., The mechanics of earthquake rupture, in *Proceedings of the International School of Physics, 'Enrico Fermi,' Course LXXVIII on Physics of the Earth's Interior*, edited by E. Boschi, North-Holland, Amsterdam, in press, 1981.

Scholz, C. H., and J. T. Engelder, The role of asperity indentation and ploughing in rock friction, I, Asperity creep and stick-slip, *Int. J. Rock Mech. Mining Sci. Geomech. Abstr.*, *13*, 149-154, 1976.

Scholz, C. H., P. Molnar, and T. Johnson, Detailed studies of frictional sliding of granite and implications for the earthquake mechanism, *J. Geophys. Res.*, *77*, 6392–6406, 1972.

Solberg, P., and J. Byerlee, Strain-rate dependent strain hardening and experimental fault creep (abstract), *Eos Trans. AGU*, *60*, 956, 1979.

Solberg, P. H., D. A. Lockner, R. S. Summers, J. D. Weeks, and J. D. Byerlee, Experimental fault creep under constant differential stress and high confining pressure, *Proc. U.S. Symp. Rock Mech. 19th*, 118–120, 1978.

Summers, R., and J. Byerlee, A note on the effect of fault gouge composition on the stability of frictional sliding, *Int. J. Rock Mech. Mining Sci. Geomech. Abstr.*, *14*, 155–160, 1977.

Tchalenko, J. S., Similarities between shear zones of different magnitude, *Geol. Soc. Am. Bull.*, *81*, 1625–1640, 1970.

Teufel, L. W., and J. M. Logan, Effect of shortening rate on the real area of contact and temperatures generated during frictional sliding, *Pure Appl. Geophys.*, *116*, 840–865, 1978.

Weeks, J., and J. Byerlee, Preliminary investigation of volume changes in crushed granite preceding stick-slip failure, *Geophys. Res. Lett.*, *5*, 832–834, 1978.